Absence of Structure Resonances in SIS100 Tune Quadrant for Heavy Ion Fast Extraction

Adrian Oeftiger*
GSI Helmholtzzentrum für Schwerionenforschung GmbH, Darmstadt, Germany
20 October 2021

GSI Report: GSI-2021-01126

Abstract: The understanding and avoidance of space charge induced resonances is of utmost importance for long storage times in synchrotrons, as they can lead to halo generation and subsequent beam loss. This report discusses the absence of structure resonances for heavy-ion operation in SIS100 in the tune quadrant foreseen for the fast extraction mode, $18.5 < Q_{x,y} < 19$. Simulations of beam losses for the duration of the SIS100 accumulation plateau at nominal transverse space charge conditions with a maximum tune shift of $\Delta Q_y^{SC} = -0.3$ supplement the discussion.

1 Setup of Beam Dynamics Simulations

The full beam dynamics simulations of a single bunch in SIS100 with nonlinear space charge, nonlinear thin-lens tracking and nonlinear RF bucket are carried out using the open source CERN code SixTrackLib [1, 2, 3]. The full SIS100 lattice [4] is simulated based on the heavy-ion fast extraction tune settings, where the working point is scanned in 0.01 intervals across the tunes $18.55 \leq Q_{x,y} < 19$. The perturbation by the two normal-conducting radiation-hardened quadrupole magnets in the extraction insertion section will be mitigated by means of the

*a.oeftiger@gsi.de

SIS100 quadrupole corrector magnets to minimise the implied gradient error. To simplify the setup, the lattice is assumed to perfectly satisfy the $S = 6$ super-periodicity and all quadrupole magnets are taken to be of the cold, super-conducting type.

All beam and machine parameters are listed in Table 1.1.

Table 1.1: Parameters for Uranium-238 Beam Production in SIS100.

Parameter	**Value**
Horizontal normalised rms emittance ϵ_x	5.9 mm mrad
Horizontal geometric KV emittance	35 mm mrad
Vertical normalised rms emittance ϵ_y	2.5 mm mrad
Vertical geometric KV emittance	15 mm mrad
Rms bunch length σ_z	13.2 m
Rms momentum deviation $\sigma_{\Delta p/p_0}$	0.44×10^{-3}
Bunch intensity N of U^{28+}_{238}	0.625×10^{11}
Max. space charge tune shift ΔQ_y^{SC}	-0.30
Chromatic tune spread $Q'_{x,y}\sigma_{\Delta p/p_0}$	0.02
RF voltage (single-harmonic) V_{RF}	58.2 kV
Harmonic h	10
Kinetic energy	$E_{kin} = 200$ MeV/u
Relativistic β factor	0.568
Revolution frequency f_{rev}	157 kHz

The simulations sample the bunch with 1000 macro-particles using an optics-matched 6D Gaussian phase space distribution. This bunch is tracked through the synchrotron elements and space charge nodes, 501 of which are placed in intervals of slightly varying length along the ring. Using more space charge nodes or more macro-particles does not significantly alter the simulation results. Space charge is modelled as fixed (i.e. non-adaptive) frozen 3D Gaussian field maps which remain constant throughout the simulation, following the formula by Bassetti and Erskine [5, 6]. The transverse beam size used in the field maps at each space charge node follows the computed local β- and dispersion functions and is based on the initial transverse emittances. The transverse nonlinear space charge force is modulated with the longitudinal Gaussian beam profile. Evaluating the initial tune footprint in the simulation gives a maximum space charge tune shift from the bare working point in the vertical plane of $\Delta Q_y^{SC} = -0.3$ for the particles in the centre of the bunch.

2 Simulations Results

In a first baseline check, the storage of a zero-current beam in the symmetric lattice is simulated for the duration of the 1 s injection plateau. The scanned tune quadrant exhibits zero beam loss and constant rms emittances – in line with the absence of external resonance driving terms in the symmetric ideal lattice.

In a next step we include the fixed frozen space charge ("FFSC") model in the simulations. Simulating again the injection plateau duration in the symmetric lattice with FFSC for bunches of nominal intensity, the Montague stop-band [7] appears around the coupling line $Q_x = Q_y$ as seen in Fig. 2.1.

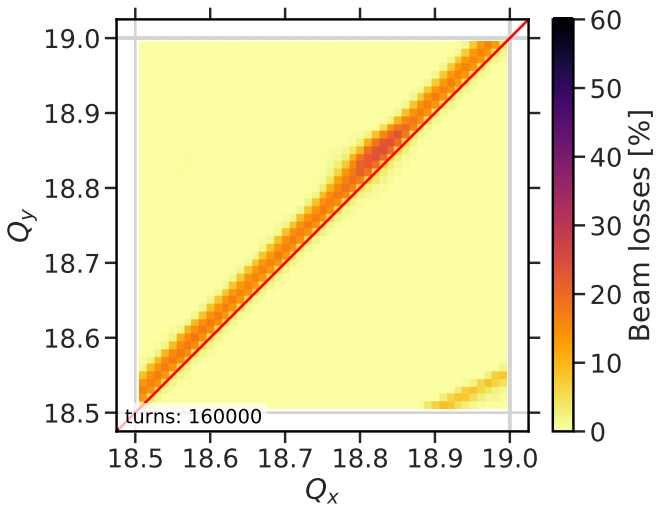

Figure 2.1: Symmetric cold lattice. Tune diagram with beam loss from FFSC simulations.

It is important to note that no other resonances significantly limit the present tune quadrant based on the symmetric lattice. The reason lies in the absence of low-order structure resonances crossing through the tune quadrant as opposed to e.g. the SIS18 ring [8]. This statement will be discussed in the following.

3 Single-particle Resonance Condition

The general (zero intensity) tune condition for betatron resonance [9] reads

$$k\,Q_x + \ell\,Q_y = m \tag{3.1}$$

for integer $k, \ell, m \in \mathbb{Z}$. The order of the resonance is given by $n \doteq |k| + |\ell|$ while m marks the harmonic driving the resonance. Systematic structure resonances are resonances with a driving harmonic m amounting to a multiple integer of structural symmetries in the ring lattice, such as the super-periodicity $S = 6$ or the 84 basic focusing cells.

Figure 3.1 shows the lines where the zero-intensity resonance condition Eq. (3.1) is satisfied, where the red colour distinguishes the structure resonances with $m = r\,S$ for integer r. Normal

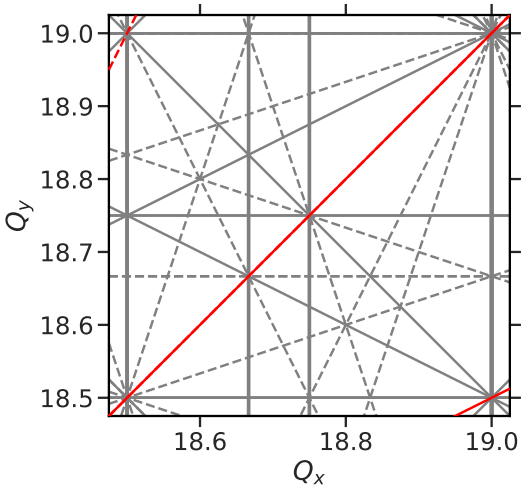

(a) Up to octupolar order $n \leq 4$.

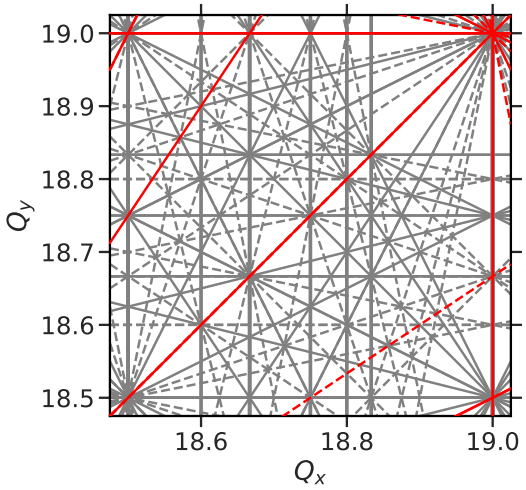

(b) Up to dodecapolar order $n \leq 6$.

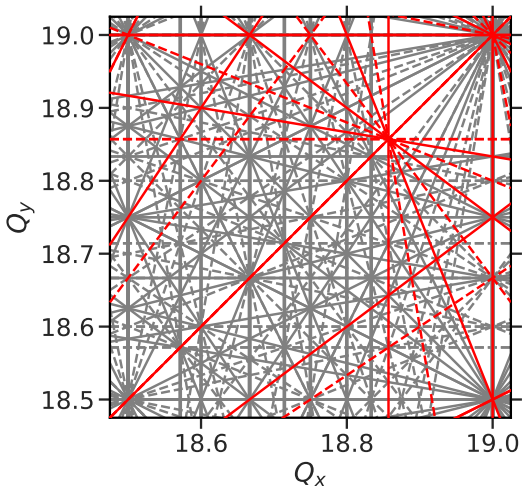

(c) Up to order $n \leq 7$.

Figure 3.1: Resonance diagram for SIS100 with super-periodicity $S = 6$ according to the single-particle Eq. (3.1).

resonances driven by b_n are plotted as solid lines, skew resonances driven by a_n as dashed lines. A normal and skew sextupole structure resonance appear on the periphery in the tune quadrant, going through $(Q_x, Q_y) = (19, 18.5)$ and $(18.5, 19)$, respectively. For decapolar order $n = 5$ we find one normal and one skew structure resonance above and below the coupling line, crossing further inside the tune diagram. Then, from order $n = 7$ on and higher, the resonance diagram is crossed by many structure resonances. Generally speaking it holds that the higher the order n, the weaker the resonance impact for equally strong a_n, b_n.

4 Incoherent vs. Coherent Resonances

The FFSC model can only predict incoherent resonances as the tracked particles cannot establish phase coherence. For the considered SIS100 tune quadrant this is sufficient: coherent resonance phenomena appear to be irrelevant in the search for resonance-free areas, as the PIC simulations in [10, Fig. 7a] demonstrate. In the following, we give a brief overview why this approach should suffice for typical situations in most space charge limited synchrotrons.

It is well known that space charge modifies the betatron resonance conditions Eq. (3.1) as recently discussed e.g. in [11] and references therein. The particles experience a defocusing effect of the transverse space charge forces which imprints as an additional detuning term $\Delta Q_{x,y}^{SC}$ in this *incoherent* resonance condition. Furthermore, the space charge force leads to inter-particle communication and the particle distribution becomes sensitive to the excitation of coherent modes. The coherent resonance condition of the corresponding bunch mode tunes involves intensity dependent $\mathscr{C}_n$ factors [12], e.g. for a vertical nth order coherent resonance as

$$n\left(Q_y - \mathscr{C}_n \left|\Delta Q_y^{KV}\right|\right) = m \quad , \tag{4.1}$$

with the rms-equivalent Kapchinskij-Vladimirskij (KV) tune shift ΔQ_y^{KV} [13],

$$Q_y^{KV} = -\frac{K^{SC} R^2}{4\sigma_y(\sigma_x + \sigma_y) Q_{y0}} \quad , \tag{4.2}$$

where K^{SC} is the space charge perveance, R the effective synchrotron radius, $\sigma_{x,y}$ the average rms beam sizes in the transverse plane and Q_{y0} the bare tune.

The structure resonance condition of integral $m = r\,S$ (where $r \in \mathbb{Z}$) for external driving terms translates to internally driven parametric resonance in the presence of space charge. They can have a severe impact on beam quality when a pumped instability occurs. For the pure alternate gradient focusing (without space charge) this parametric resonance mechanism is known from the single-particle 180° or Mathieu instability. For finite space charge also lower phase advance than 180° per cell can lead to parametric resonance, specifically when coherent beam modes become unstable. An important feature of the parametric resonance condition is that this instability occurs twice as dense in tune space compared to the regular resonances in Eqs. (3.1) and (4.1), namely at half-integer harmonics $m \mapsto \frac{m}{2}$. While in parametric resonance research this insight goes as far back as to the 19th century (cf. e.g. Ref. [14]), the occurrence of the $m/2$ condition in intense beam dynamics is known at least since Ref. [15].

Recently, Ref. [16] argued that the 2D resonance diagram should be constructed entirely based on parametric coherent resonances including the nonlinear orders, which would mean twice as many red lines in Fig. 3.1, based on the half-integer harmonic condition $\frac{m}{2} = r\,S$. Fortunately, for Gaussian bunch distributions in alternate gradient focusing, parametric coherent resonance occurs only for the second-order $n = 2$ case (also called the envelope instability). As noted for 1D in Ref. [17] and for 2D (and bunched beam) in Ref. [11], nonlinear orders $n \geq 3$ are Landau damped. Therefore, higher-order parametric coherent resonances seem to be generally absent for realistic beam conditions.

For SIS100 with $S = 6$, the nearest $n = 2$ parametric coherent resonance stop-bands are located close to (above) $Q_{x,y} = 18$ and $Q_{x,y} = 19.5$, and thus far away from the design tune quadrant $18.5 \leq Q_{x,y} \leq 19$ for fast extraction of heavy-ion beams. Even when searching for loss-free working points close to such an envelope instability stop-band, the results of Ref. [11] show that the incoherent 4th order stop-band overlaps and entirely embraces the coherent one – both on the lower end (halo tune region) and the higher end (outer core tune region). The bunched beam FFSC predictions are found to correctly identify the resonance-free tune space.

Also in the absence of parametric coherent resonance (e.g. due to Landau damping), structure resonances at integer harmonics $m = r\,S$ can be harmful: the incoherent resonance mechanism can generally lead to halo formation and eventual beam loss. Driving terms can be provided externally (e.g. regularly spaced sextupole magnets) or internally (e.g. space charge). In the latter case, the modulation of the space charge potential along the alternate gradient focusing provides resonance driving terms for all even-order $k, \ell = 0, 2, 4, \ldots$ in Eq. (3.1). Large-amplitude particles meeting this incoherent resonance condition are excited and potentially driven into the machine aperture. The CERN Proton Synchrotron is an example for space charge limitation by the halo generation through an 8th order structure resonance [18], demonstrating that even very high orders (which are usually disregarded) can be detrimental.

In summary, these incoherent resonance mechanisms for halo and outer core are caught by the FFSC model when using realistic lattices. It is very useful to understand that computational prediction of the location of incoherent space charge driven stop-bands with FFSC are hence not only valid, but even a viable means to identify the edges of resonance-free areas.

5 Identifying the Incoherent Space Charge Driven Resonances in SIS100

We turn our attention back to the SIS100 FFSC simulations presented in Fig. 2.1. Driving terms for nonlinear resonances are solely provided by the space charge potential, where the harmonic m is determined by the beam size modulation given by the structure of the lattice. To stress it once more, only structure resonances with even k, ℓ can therefore appear in the tune diagram. The predicted beam loss appearing in Fig. 3.1a close to the third-order structure resonance $Q_x - 2Q_y = -18$, which touches the tune quadrant at $Q_x = 19$ and $Q_y = 18.5$, is in reality induced by the coinciding sixth-order structure resonance

$$2Q_x - 4Q_y = -36 = -6 \cdot S \quad . \tag{5.1}$$

The next higher-order structure resonances in Fig. 3.1b are the decapolar ones: the normal one above the coupling line, satisfying $3Q_x - 2Q_y = 18$, shows nearby weak rms emittance exchange as well as minimal loss on the 1% level in the FFSC simulations. Again, the actual reason for the observed dynamics is the space charge driven 10th order structure resonance

$$6Q_x - 4Q_y = 36 = 6 \cdot S \quad . \tag{5.2}$$

Its effect of ≈ 1% beam loss is already too weak to appear on the beam loss scale shown in Fig. 2.1.

Figure 5.1 shows the same beam loss results with a smaller scale of up to 5% beam loss, with the two observed space charge driven structure resonances indicated in red. Further very low losses are visible here along the 14th order resonance lines. However, all these high-order resonances with 1% beam loss and less play no role in realistic scenarios including the magnet imperfection driven resonances – compare e.g. to FFSC simulations with the SIS100 field error model as presented in [10, Fig. 7a], where the usual externally driven resonances simply overshadow the 10th order space space charge driven resonances given the SIS100 design beam parameters.

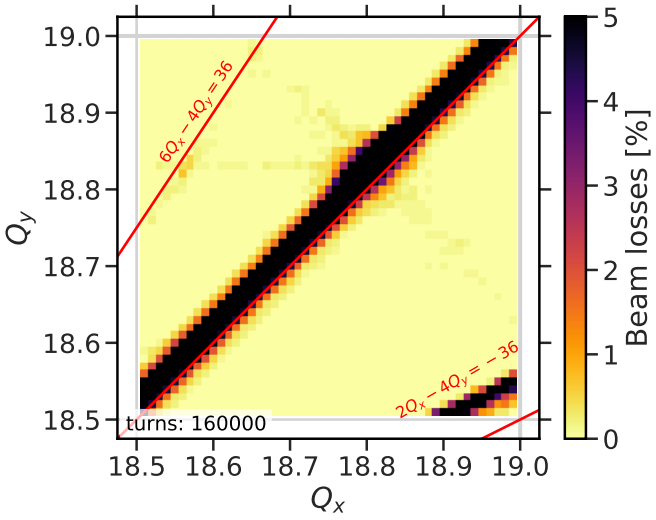

Figure 5.1: Same as Fig. 2.1 with structure resonances indicated.

6 Conclusion

All in all, from the optics design point of view, one should avoid tune quadrants with structure resonances to push the space charge limit in synchrotrons with an accumulation plateau. At the same time, it is not necessary to consider half-integer harmonics for structure resonances due to the parametric coherent resonances – one can resort to the usual incoherent resonance diagrams to at least 6th order. The incoherent stopbands will embrace and include the coherent stopbands as long as the space charge induced tune spread remains unmodified

(which can happen e.g. due to nonlinear electron lenses). The lesson learned is that it is sufficient to search for incoherent resonance phenomena with fixed frozen space charge models in order to correctly identify resonance-free areas.

References

[1] M. Schwinzerl, R. De Maria, K. Paraschou, H. Bartosik, G. Iadarola, and A. Oeftiger. "Optimising and Extending a Single-particle Tracking Library for High Parallel Performance". In: *Proceedings of the 12th International Particle Accelerator Conference*. 2021, THPAB190.

[2] R. De Maria et al. "SixTrack V and runtime environment". In: *International Journal of Modern Physics A* 34.36 (2019), p. 1942035.

[3] M. Schwinzerl et al. *SixTrackLib*. `https://github.com/SixTrack/sixtracklib/tree/6893b94f4e872a89869bcdecef91f15648b4cc21`. 2020.

[4] Y. El Hayek and D. Ondreka. *SIS100 optics*. `https://git.gsi.de/sys/lattices/-/tree/c372947cfd39719efffda9fbce810fae189857fb`. 2020.

[5] M Bassetti and George A Erskine. *Closed expression for the electrical field of a two-dimensional Gaussian charge*. Tech. rep. CERN-ISR-TH-80-06. Geneva: CERN, 1980. URL: `https://cds.cern.ch/record/122227`.

[6] Adrian Oeftiger et al. "Review of CPU and GPU Faddeeva Implementations". In: *Proceedings of the 7th International Particle Accelerator Conference*. CERN-ACC-2016-193. 2016, WEPOY044. DOI: `10.18429/JACoW-IPAC2016-WEPOY044`. URL: `https://cds.cern.ch/record/2207430`.

[7] Brian William St Leger Montague. *Fourth-order coupling resonance excited by space-charge forces in a synchrotron*. Tech. rep. CERN-1968-038. Geneva: CERN, 1968.

[8] I Hofmann, G Franchetti, and A Fedotov. "Space charge resonances and instabilities in rings". In: *Proceedings of the 20th ICFA Advanced Beam Dynamics Workshop on High Intensity and High Brightness Hadron Beams, Batavia, Illinois*. 2002, p. 248.

[9] Ernest D Courant and Hartland S Snyder. "Theory of the alternating-gradient synchrotron". In: *Annals of physics* 3.1 (1958), pp. 1–48.

[10] Adrian Oeftiger, Oliver Boine-Frankenheim, Vera Chetvertkova, Vladimir Kornilov, Dmitrii Rabusov, and Stefan Sorge. "Simulation Study of the Space Charge Limit for the FAIR Heavy-ion Synchrotron SIS100". In: *to be published* (2022).

[11] Ingo Hofmann, Adrian Oeftiger, and Oliver Boine-Frankenheim. "Self-consistent long-term dynamics of space charge driven resonances in 2D and 3D". In: *Phys. Rev. Accel. Beams* 24 (2 Feb. 2021), p. 024201. DOI: `10.1103/PhysRevAccelBeams.24.024201`. URL: `https://link.aps.org/doi/10.1103/PhysRevAccelBeams.24.024201`.

[12] Richard Baartman. "Betatron resonances with space charge". In: *AIP Conference Proceedings*. Vol. 448, No. 1. American Institute of Physics. 1998, pp. 56–72.

[13] IM Kapchinskij and VV Vladimirskij. “Limitations of proton beam current in a strong focusing linear accelerator associated with the beam space charge”. In: *Proceedings of the International Conference on High Energy Accelerators and Instrumentation*. CERN Scientific Information Service Geneva. 1959, p. 274.

[14] Lord Rayleigh. “XVII. On the maintenance of vibrations by forces of double frequency, and on the propagation of waves through a medium endowed with a periodic structure”. In: *The London, Edinburgh, and Dublin Philosophical Magazine and Journal of Science* 24.147 (1887), pp. 145–159.

[15] I Hofmann, L J Laslett, L Smith, and I Haber. “Stability of the Kapchinskij-Vladimirskij (K-V) distribution in long periodic transport systems”. In: *Part. Accel.* 13.LBL-14922 (Aug. 1982), 145–178. 61 p. URL: https://cds.cern.ch/record/140869.

[16] K. Kojima, H. Okamoto, and Y. Tokashiki. “Empirical condition of betatron resonances with space charge”. In: *Phys. Rev. Accel. Beams* 22 (7 July 2019), p. 074201. DOI: 10.1103/PhysRevAccelBeams.22.074201. URL: https://link.aps.org/doi/10.1103/PhysRevAccelBeams.22.074201.

[17] H. Okamoto and K. Yokoya. “Parametric resonances in intense one-dimensional beams propagating through a periodic focusing channel”. In: *Nucl. Instrum. Meth. A* 482 (2002), pp. 51–64. DOI: 10.1016/S0168-9002(01)01684-9.

[18] F. Asvesta et al. “Identification and characterization of high order incoherent space charge driven structure resonances in the CERN Proton Synchrotron”. In: *Phys. Rev. Accel. Beams* 23 (9 Sept. 2020), p. 091001. DOI: 10.1103/PhysRevAccelBeams.23.091001. URL: https://link.aps.org/doi/10.1103/PhysRevAccelBeams.23.091001.